Desalination and Water Treatment
www.deswater.com

doi:10.5004/dwt.2018.22157

107 (2018) 324–331
March

TiO_2 nanosheet incorporated polysulfone ultrafiltration membranes for dye removal

Abhinav K. Nair, B. Vinay Kumar, Gopinath Kalaiarasan, P.E. Jagadeesh Babu*

Department of Chemical Engineering, National Institute of Technology Karnataka, Surathkal, Mangalore 575 025, India, Tel. +91 8792706002, email: abhinav2411@yahoo.com (A.K. Nair), Tel. +91 8242474000, email: vinay3968@gmail.com (B.V. Kumar), Tel. + 91 8242474000, email: gopinath075@gmail.com (G. Kalaiarasan), Tel. +91 8242474000, Fax +91 08242474057, email: dr.jagadeesh@yahoo.co.in, jagadeesh78@nitk.ac.in (P.E. Jagadeesh Babu)

Received 28 March 2017; Accepted 4 March 2018

ABSTRACT

Incorporation of nanomaterials in polymeric membranes is an effective means to improve membrane performance. In the present work, a novel additive TiO_2 nanosheet was incorporated in polysulfone membrane. TiO_2 nanosheets were synthesised by hydro-thermal method and blended with polysulfone to give nanocomposite membranes. The membranes performance was evaluated via pure water flux, bovine serum albumin rejection and anti fouling studies. Further the membranes were subjected to dye rejection application using Congo red and Rhodamine-B dyes. The membranes were characterised using scanning electron microscopy; X-ray diffraction and contact angle measurement. The nanocomposite membranes exhibited superior permeation, anti fouling and dye rejection traits.

Keywords: TiO_2 nanosheets; Polysulfone; Nanocomposite; Membrane; Dye

1. Introduction

Membrane filtration is widely used in water treatment because of its lesser energy consumption, lower installation and operation cost when compared to conventional processes [1]. Ultrafiltration is comparatively a low pressure filtration process which helps in removal of colloids, pathogens and macromolecules and thereby reducing the addition of chemicals for water treatment [2]. Polysulfone (PSF) is a good membrane material and is popularly in use for its excellent heat resistance, chemical compatibility and resistance over wide range of pH [3]. Hydrophobicity which results in low flux is the main drawback of PSF membranes,this adversely effects water treatment. Hydrophobicity also makes PSF membranes more vulnerable to fouling [4]. Addition of various hydrophilic inorganic nano additives like SiO_2, Al_2O_3, Fe_2O_3 and TiO_2 nanoparticles have shown to improve the hydrophilicity and enable better permeation properties of polymeric membranes [5–7].

In case of PSF, titanium dioxide nanomaterials have been widely reported [8,9]. So far, addition of TiO_2 nanoparticles , nanotubes and nanofibers has been reported in literature. Addition of TiO_2 nanoparticles and nanotubes at higher concentration in PSF has shown to degrade membrane performance due to delayed demixing [10,11]. Where as in our previous work with TiO_2 nanofibers in PSF and Cellulose acetate membranes the membrane properties improved significantly at higher additive content [12,13]. It is a well established fact that the morphology of nano additive significantly affects the membrane modification and performance [14]. TiO_2 nanosheets are yet another nano structure of TiO_2 that has attracted much attention recently [15]. They are 2D nano structures with thickness of few nano metres. Such nano structures are of importance due to their high surface energy and high specific surface area [16]. High specific surface area and thin sheet structure provides greater inter facial area, providing good interaction between the additive and the filler.

In this work,we report the addition of titanium dioxide nanosheets (TNS) as a novel additive in PSF membranes. To the best of our knowledge TNS as a polymer membrane additive has not been reported before. TNS were synthesized using solvo thermal route. The synthesized TNS are characterized by X-ray diffraction (XRD), scanning electron microscopy (SEM) and transmission electron microscopy

*Corresponding author.

(TEM). Later the TNS are incorporated as an additive into PSF membrane casting solution to prepare nanocomposite membranes. The performance of the membranes was evaluated in terms of pure water flux, BSA rejection and flux recovery [17]. The membranes were used for dye rejection application using Congo red and Rhodamine-B dyes as model pollutant.

2. Experimental

2.1. Materials

Tetra butyl titanate (98%), Polysulfone (PSF, M_W~35000Da), Bovine serum albumin (BSA), Rhodamine-B dye and Bradford reagent were purchased from Sigma-Aldrich Co, Bangalore, India. Hydrofluoric acid (HF, 40%) and Congo red dye powder were purchased from Nice chemicals, Kochi. 1-methyl-2-pyrrolidine (NMP) and polyethylene glycol (PEG, M_W ~ 600 Da) were purchased from Merck specialities private ltd., west Mumbai. All the chemicals were used without any further purification.

2.2. Synthesis of TNS

10 mL of tetra butyl titanate was added drop wise into a Teflon-lined stainless steel autoclave containing 3 mL of HF under magnetic stirring. The autoclave was kept at 200°C for 24 h in an electric hot air oven, then cool down naturally to room temperature. The TiO_2 sample was harvested by centrifugation, washed thoroughly with deionised water 3 times and absolute ethanol 2 times, and then dried at 50°C overnight [18,19].

2.3. Preparation of TNS incorporated PSF membranes

For preparation of M-1 membrane, PSF (20 wt. %) and NMP (80 wt. %) were mixed and stirred at 60°C over a period of 4 h for complete dissolution of PSF to obtain a homogeneous solution. 1.0 wt. % (with respect to polymer solution) of TiO_2 nanosheets (with respect to weight of polymer solution) was added to the solution at the same temperature and further stirred for 30 min. All the solutions were prepared in closed beakers to avoid evaporation of solvent. The viscous solution was cast over a glass plate using a finely polished glass rod by maintaining a membrane thickness of 0.3 mm. The glass plate was then immersed in distilled water (at 25°C) for phase inversion [20]. A similar procedure was followed for the preparation of other membranes with compositions as shown in Table 1.

Table 1
Blending compositions of membranes

Membranes	Polymer solution (PS)		TiO_2 (wt. % of PS)
	PSF (wt %)	NMP (wt %)	
M-0	20	80	0
M-1	20	80	1
M-3	20	80	3
M-5	20	80	5
M-7	20	80	7
M-10	20	80	10
M-12	20	80	12
M-15	20	80	15

3. Characterization

3.1. XRD analysis

X-ray diffraction analysis was done using goniometer (JEOL Dx-GE-2P, Japan), X-ray diffractometer equipped with monochromatised high intensity Cu Kα radiation (λ = 1.54058Å). The diffractograms were obtained at 0.16°/s in the 2θ range of 10–70°. Accelerating voltage was set to 30 kV and a current of 20 mA. XRD was used to find the crystallinity of nanosheets as well as the TNS incorporated PSF membranes.

3.2. SEM analysis

Morphologhy of synthesized nanosheets and membrane samples were analysed using SEM. The samples were frozen in liquid nitrogen and fractured before gold sputtering. Cross-sectional images of the membranes were observed with JEOL (JSM-6380LA), Scanning electron microscope.

3.3. TEM analysis

The morphology and structure of as-prepared products were examined by Transmission electron microscopy (TEM, JEOL, JEM-2100). All the TEM samples were prepared by the deposition of a drop diluted suspensions on a carbon film coated copper grid.

3.6. Contact angle measurement

FTA-200 Dynamic contact angle analyzer was used to estimate the contact angle of membranes using sessile droplet method. To avoid error three measurements were made at different locations and the average is reported.

3.4. Permeation properties

Sterlitech HP4750 stirred dead end filtration cell with an effective membrane area of 14.6 cm^2 was used to study the performance of the membranes. Membranes were kept immersed in distilled water for 24 h before carrying out flux study. The permeate sample collection was started after 20 min of exposure to 0.4 MPa transmembrane pressure (TMP) at 25°C. The flux study was conducted for a time period of 90 min to enable the flux to reach near steady state condition. The PWF (J_w) was calculated using the following equation:

$$J_w = \frac{Q}{\Delta t\, A} \tag{1}$$

where J_w is expressed in L/m^2 h and Q is the amount of water collected for Δt (h) time duration using a membrane of area A (m^2).

3.5. Anti fouling properties

The anti fouling property of the membrane was studied as per the procedure reported in literature [21]. In Brief, initial pure water flux of the membrane J_{w1} (L/m²h) was obtained at 0.4 MPa transmembrane pressure for 90 min. The anti fouling property of the membrane was studied using BSA as standard protein for rejection. 0.8 g/L of aqueous solution of BSA was prepared and filtered through the membrane for 60 min. Later the membrane was flushed with distilled water for 20 min and pure water flux J_{w2} (L/m²h) was determined once again. The membrane anti fouling property was estimated in terms of flux recovery ratio (FRR) using the following equation:

$$FRR(\%) = \frac{J_{w2}}{J_{w1}} \times 100 \quad (2)$$

In order to determine the rejection capacity of the membrane, feed and permeate solution samples were collected and treated with Bradford reagent. Blue colour solution is formed when adding Bradford reagent. Samples were kept at room temperature for 10 min before analyzing using UV-Spectrometer. Absorption peak of BSA is found to be 595 nm. The % BSA rejection of the membrane was determined using the following equation:

$$\%R = \left(1 - \frac{C_p}{C_f}\right) \times 100 \quad (3)$$

where C_p (mg/L) and C_f (mg/L) are the BSA concentrations in permeate and feed respectively. The concentrations were measured using UV-Spectrophotometer at a wavelength of 595 nm.

3.6. Dye rejection study

Congo red and Rhodamine-Bdye (50 ppm) were prepared and filtered through the membranes at 0.4 MPa trans-membrane pressure to study the dye rejection. The permeate collected was subjected to UV-Vis spectroscopy to estimate residual dye concentration at a wavelength of 498 nm and 553 nm respectively. Percentage rejection values of dye were calculated using above Eq. (3), where C_p (mg/L) and C_f (mg/L) are the dye concentrations in permeate and feed respectively.

4. Results and discussion

4.1. Characterization of TNS

The TNS synthesized are in the size range of 100–200 nm and are in rectangular shape (Fig. 1). As seen from the TEM image, TNS is semi-transparent under electron beam which indicates their thin structure with thickness of few nanometers [18]. Size distribution of TNS measured by DLS technique is shown in Fig. 2. The size distribution obtained revealed two peaks corresponding to two dimensions of the nanosheets. The smaller peak at lower intensity corresponds to the thickness had a mean value of 4.7 nm and the larger peak corresponding to the length/breadth had a mean value of 218.8 nm. The XRD pattern of TNS is shown in Fig. 3. The major XRD peaks at 25.2°, 37.72°, 47.98° and

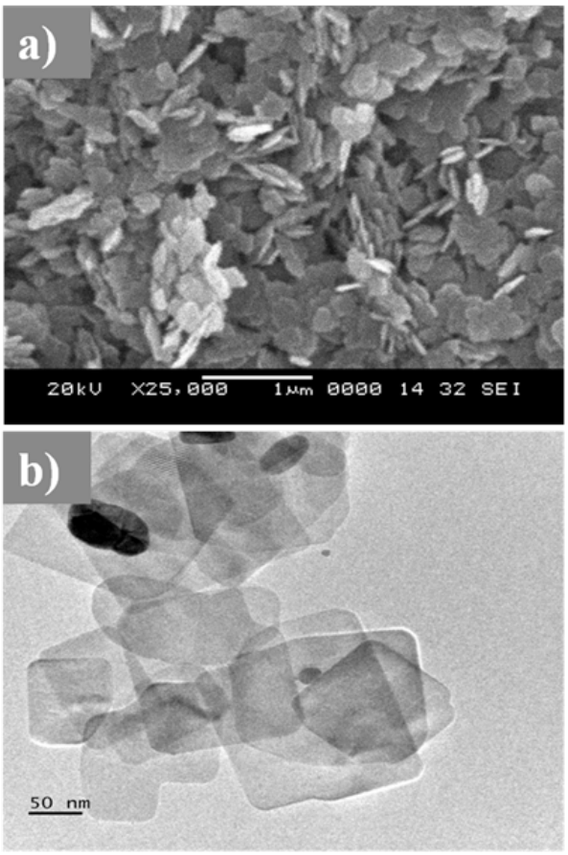

Fig. 1. a) SEM image of TNS, b) TEM image of TNS.

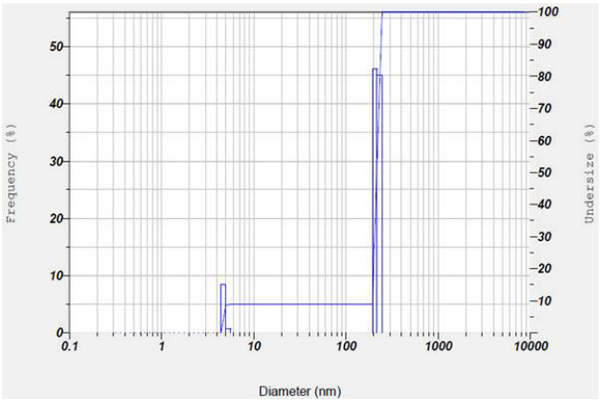

Fig. 2. Size distribution of TNS measured by DLS technique.

54.98° can be indexed to the characteristic peaks of anatase phase TiO_2 [22].

4.2. Membrane characterization

4.2.1. XRD analysis

XRD patterns of M-0, M-10 and TNS are compared in Fig . 3. The major anatase peaks observed in TNS are

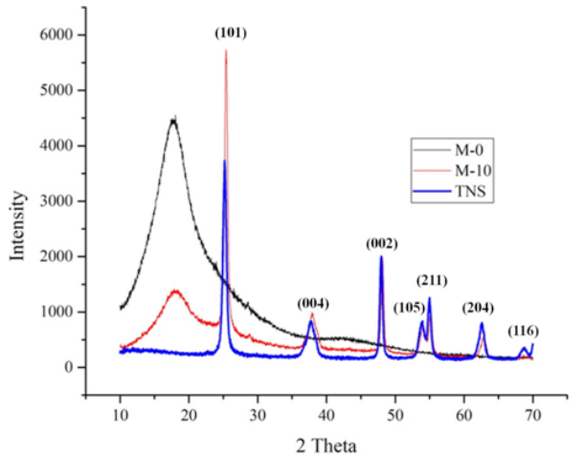

Fig. 3. XRD patterns of M-0, M-10 and TNS.

also observed in M-10 membrane, which shows that TNS were incorporated into membranes effectively. M-0 pattern does not give any characteristic sharp peaks which indicate amorphous polysulfone, without any crystalline phase [23].

4.2.2. Morphology of the membranes

Cross-section of the membranes synthesized with different concentrations of TNS were analysed using SEM and is shown in Fig. 4. All the membranes have typical a symmetric structure with finger like macro voids in macro pore region, less porous sub layer formation and top layer with less pore density [24]. As the TNS concentration increased from 1 wt. % to 5 wt. % the presence of micro passages in top layer and macro voids in macro pore region have decreased rapidly. With addition of particulates, viscosity of the casting solution increases which

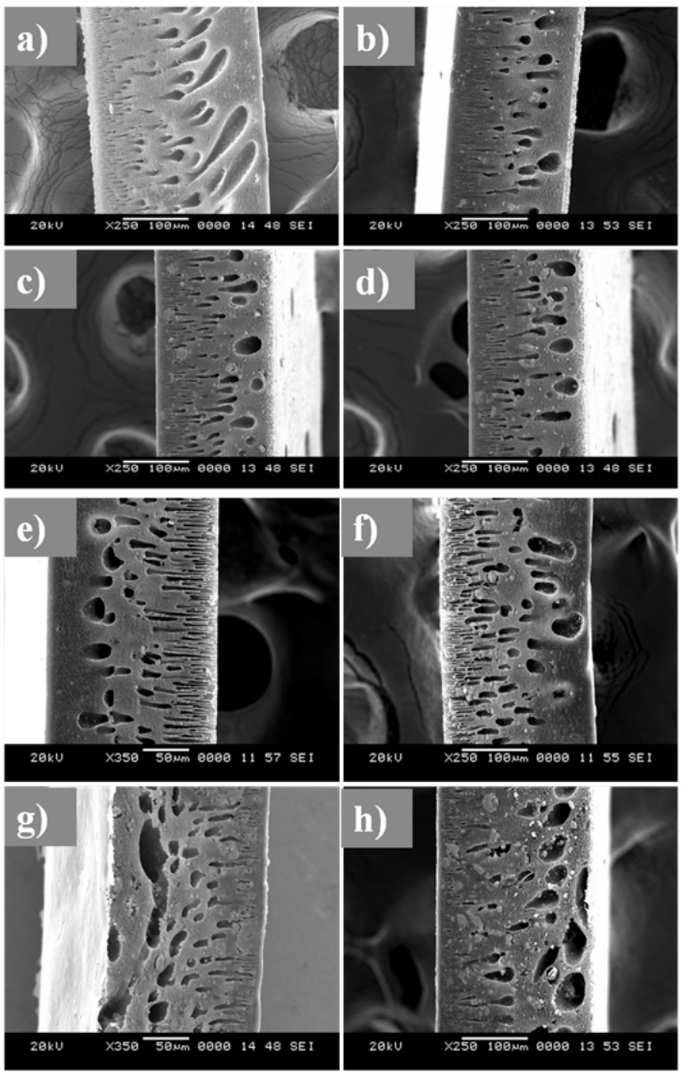

Fig. 4. SEM images of the membranes. a) M-0, b) M-1, c) M-3, d) M-5, e) M-7, f) M-10, g) M-12, and h) M-15.

delays demixing process thereby retarding rapid exchange of solvent and non-solvent. Delayed demixing results in membrane with dense skin layer and porous sub-layer [25]. From 7 wt. % TNS addition onwards porous sub layer formation becomes significant and was predominant in 12 and 15 wt.%. In M-12 and M-15 membranes, porous sub layer and macro voids regions have merged. Also the macro voids and spongy sub layer increased significantly in case of M-12 and M-15, when compared to other membranes. With increase in hydrophilic TNS concentration, the affinity of membrane towards water increases. This favours the in-diffusion of non-solvent in to the membrane. This can help in overcoming the viscosity barrier and results in greater porosity [20]. This is evident from the better pore formation in porous sub layer and macro void region for membranes above 7 wt.% TNS content. Better water affinity of membrane due to greater hydrophilic additive can thus enhance phase inversion and produce membranes with slightly higher pore size. From the SEM images, it appears that up to 5 wt. % of TNS addition the porosity has decreased. The addition of TNS and subsequent hydrophilicity enhancement could not significantly enhance the kinetics of phase inversion up to 5wt.%. For 7 wt % and above, the appreciable number of macro voids and pores indicate that phase inversion rate was improved due to addition of hydrophilic TNS. [26].

Surface images of the membranes obtained from FESEM analysis is shown in Fig. 5. The M-0 membrane is seen to posses very few number of pores on the surface. In case of M-5 no pores can be seen on the surface of the membrane. Whereas, in case of M-10 and M-12 membranes large number of pores can be seen and very high increase in the porous structure is observed. This clearly concurs with the observation made in the cross-sectional analysis of the membranes. The porous nature of the membranes has decreased in case of M-5 and thereafter increased, with a maximum in case of M-15 (Fig. 5(d)).

4.2.3. Hydrophilicity of membranes

Contact angle measurement can evaluate the hyphilicity of membranes. If the hydrophilicity is high, interaction between water and membrane surface is high, which is a desirable criterion for achieving high flux and anti fouling property. Fig. 6 shows contact angle measurement of the synthesised membranes. With increased addition of hydrophilic TNS, contact angle of membranes decreased from 75.04 for nascent PSF to M-15 with a lowest of 61.25. M-5 membrane showed higher contact angle compared to M-0 membrane indicating lower pore size as seen from the FESEM surface images. The decrease in contact angle of the membranes above 7 wt. % TNS content can be attributed to the presence of hydrophilic TNS of membrane surface and also the increasing pore size of the membrane [27].

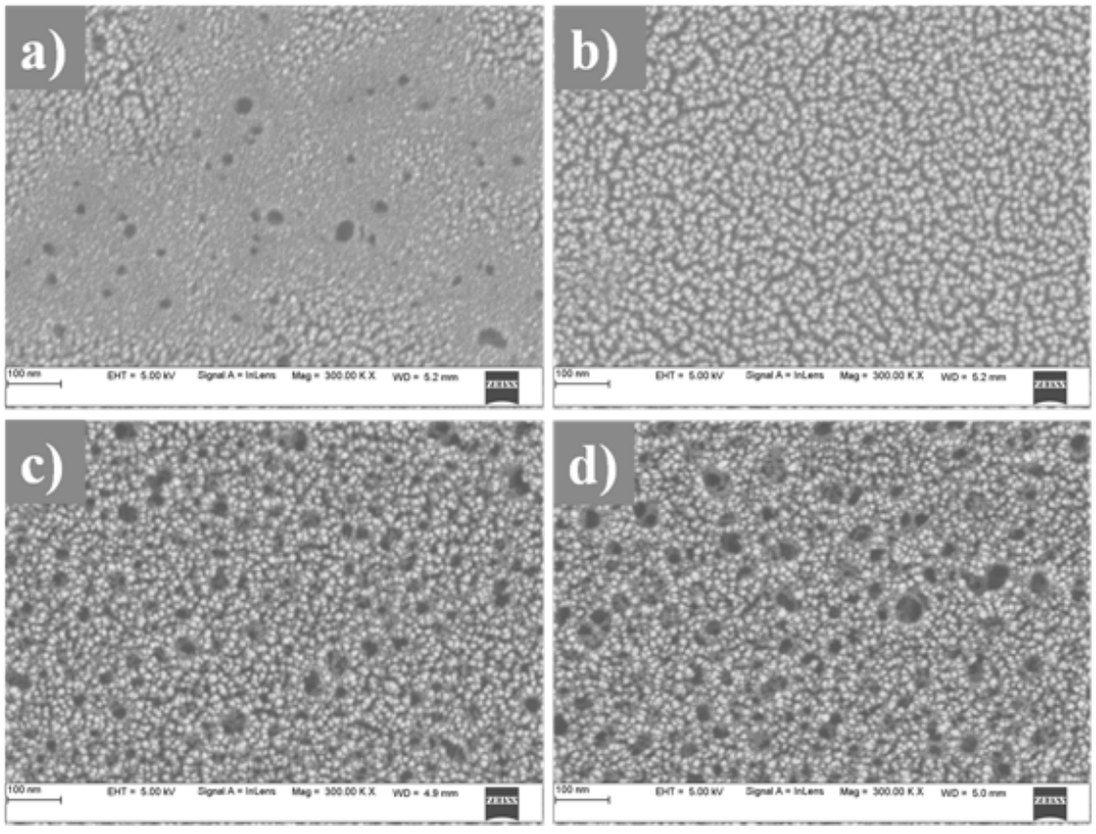

Fig. 5. FESEM images of the membrane surfaces. a) M-0, b) M-5, c) M-10, d) M-15.

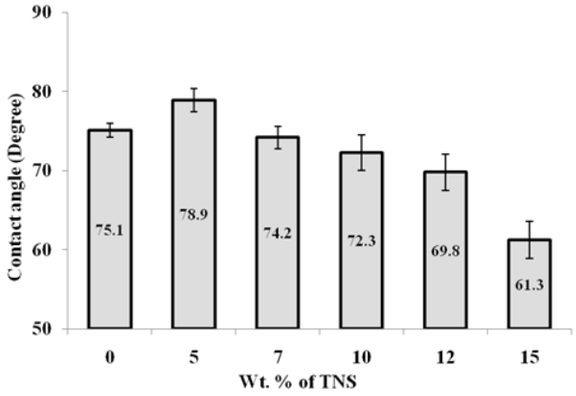

Fig. 6. Contact angle measurement of membranes.

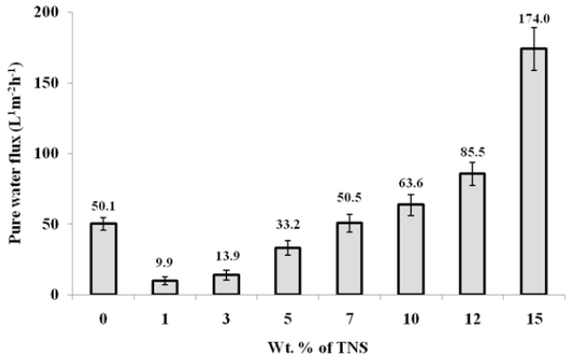

Fig. 7. PWF trend of membranes.

4.2.4. Membrane permeability and anti fouling properties

The PWF study results of the membranes are shown in Fig. 7. It was observed that the increase in TNS concentration has increased pure water flux, except at lower concentrations in case of M-1, M-3 and M-5 membranes. The decrease in flux is due to low porosity compared to M-0 membrane. The low pore size is due to increase in viscosity of casting solution (acts as frictional barrier) which effects the mutual diffusivities of solvent and non solvent during phase inversion process eventually forming a closed structure with lesser pore volume relatively [28]. M-1 and M-3 are not considered for further study because of their poor flux. The decreasing flux for M-5 membrane can be assumed from the lower contact angle. The increasing PWF trend from 7 wt. % TNS can be attributed to increase in hydrophilic nature of membranes and porosity with TNS addition. M-15 exhibited three times higher flux than nascent PSF because of high hydrophilicity and increase in sponginess of membrane.

BSA rejection study was carried out to estimate the anti fouling properties of the membranes. Fouling reduces the rejection flux due to cake layer formation and increased resistance. The same trend is observed here as shown in Fig. 8. The BSA rejection flux drastically decreased when compared to PWF, but the rejection flux improved comparatively at higher TNS content in the membranes. The BSA rejection values of the membranes are shown in Fig. 7. The maximum rejection of 96.45% was obtained for M-5 membrane due to low porosity compared to M-0 membrane. With addition of TNS the rejection values decreased and M-15 gave lowest rejection and the highest flux. With increase in TNS concentration the FRR value increased compared to M-0 membrane (Fig. 9). The increasing trend was followed till M-12 membrane and later it decreased for M-15 membrane. The maximum FRR value was observed for M-12 membrane. The interaction with the aqueous medium was enhanced with presence of hydrophilic TNS on membrane surface there by weakening the interactions between protein molecules and membrane surface. Because of weaker interactions, the foulant can be easily cleaned from membrane surface and thus increasing the longevity of membrane [29]. However, the decrease in FRR value for M-15 membrane indicates irreversible fouling. The protein molecules penetrated into

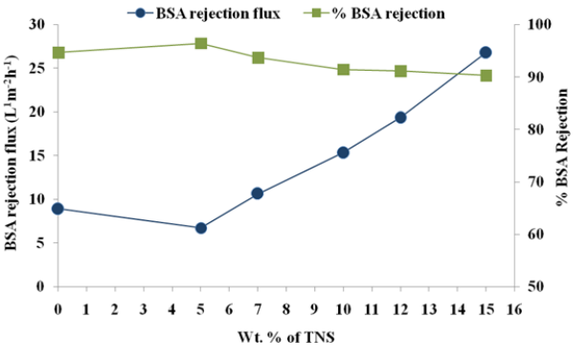

Fig. 8. BSA rejection studies of membranes.

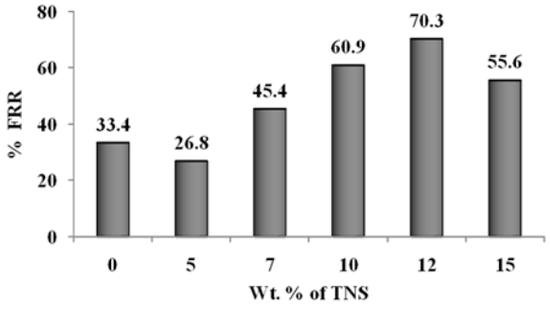

Fig.9. Percentage FRR of membranes.

membrane pores instead of superficial deposition on the membrane, thereby reducing the flux recovery.

4.2.5. Dye rejection

The Congo red dye rejection trends of the membranes are shown in Fig. 10. All TNS incorporated membranes showed better Congo red dye rejection than nascent PSF, above 90%. Although M-5 showed high dye rejection the permeate flux obtained was comparatively lower. M-12 and M-15 membranes exhibited good dye rejection along with permeate fluxes 5–6 times higher than M-0. Although

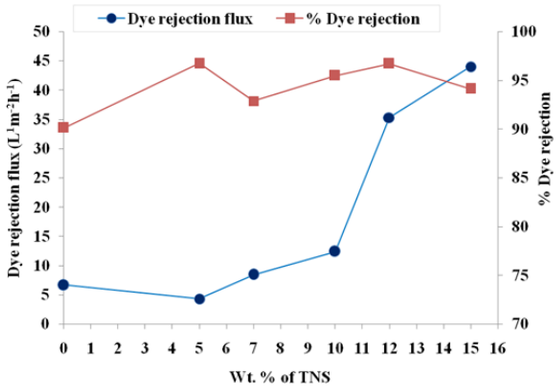

Fig. 10. Congo red dye rejection studies of membranes.

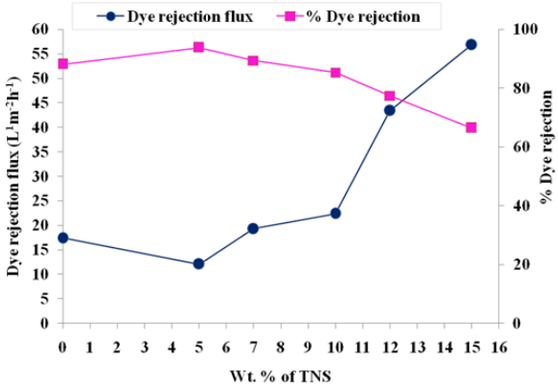

Fig. 11. Rhodamine-B dye rejection studies of membranes.

a slight decreasing trend in dye rejection was observed from M-5 to M-7, Congo red dye adsorption capability of TNS increased the rejection at higher TNS content in membranes [30,31]. Rhodamine-B dye rejection trends are shown in Fig. 11. All membranes showed better permeate flux and lower rejection for Rhodamine-B when compared to Congo red owing to the comparatively smaller size of Rhodamine-B molecules. Similar to Congo red rejection study, M-5 membrane exhibited better rejection but permeate flux was low. The permeate flux improved gradually from M-7 to M-10 and drastic increase was observed for M-12 and M-15. The drastic hike in permeate flux of M-12 and M-15 was associated with a heavy drop in dye rejection capacity, M-15 showed a minimum dye rejection of 66.4%. M-7 and M-10 membranes exhibited better performance with dye rejections above 85% dye rejection and better permeate flux.

5. Conclusion

TiO_2 Nanosheets were successfully synthesized and effectively incorporated in polysulfone membrane. The performance of the membranes showed a declining trend at lower additive concentration up to 5 wt.%, but at higher concentrations property enhancement was significant. Three times increase in pure water flux when compared to nascent polysulfone was observed for M-15 membrane. A maximum of 70.3% flux recovery was obtained for M-12 membrane, owing to the drastic increase in membrane hydrophilicity due to TNS addition. Better Congo red dye dye rejection flux was also obtained with higher TNS content. Best results for Congo red dye rejection were obtained for M-12 and M-15 membranes with dye rejection above 94% and 5–6 times increase in permeate flux. In case of Rhodamine-B rejection, the smaller size of the dye resulted in higher permeate flux accompanied by decrease in dye rejection. M-7 and M-10 membranes were found optimal for Rhodamine-B rejection, with dye rejections above 85% and comparatively higher permeate fluxes. In summary TNS could effectively enhance the overall performance of the membrane. Good dye rejection characteristics of the TNS incorporated membranes indicate potential application in membrane assisted photo catalysis.

Acknowledgements

The authors thank Prof. K. Narayan Prabhu, Metallurgical and Materials Engineering Department of NITK Surathkal, India for providing contact angle measurement facility.

References

[1] A.K. Nair, P.E. JagadeeshBabu, Ag-TiO_2 nanosheet embedded photocatalytic membrane for solar water treatment, J. Environ, Chem. Eng., 5 (2017) 4128–4133.
[2] H. Sofiah, A. Asmadi, A. Endut, Preparation and characterization of a polysulfone ultrafiltration membrane for bovine serum albumin separation : Effect of polymer concentration, Desal. Water Treat., 32 (2011) 248–255.
[3] P. Moradihamedani, A. Halim, B. Abdullah, Phosphate removal from water by polysulfone ultrafiltration membrane using PVP as a hydrophilic modifier, Desal. Water Treat., 3994 (2016).
[4] Y. Ma, F. Shi, J. Ma, M. Wu, J. Zhang, C. Gao, Effect of PEG additive on the morphology and performance of polysulfone ultrafiltration membranes, Desalination, 272 (2011) 51–58.
[5] A.L. Ahmad, M.A. Majid, B.S. Ooi, Functionalized PSf/SiO_2 nanocomposite membrane for oil-in-water emulsion separation, Desalination, 268 (2011) 266–269.
[6] M. Homayoonfal, M.R. Mehrnia, M. Shariaty-Niassar, A. Akbari, M.H. Sarrafzadeh, A. Fauzi Ismail, Fabrication of magnetic nanocomposite membrane for separation of organic contaminant from water, Desal. Water Treat., 54 (2015) 3603–3609.
[7] Y. Zhang, X. Shan, Z. Jin, Y. Wang, Synthesis of sulfated Y-doped zirconia particles and effect on properties of polysulfone membranes for treatment of wastewater containing oil, J. Hazard. Mater., 192 (2011) 559–567.
[8] M.M. Mahlambi, G.D. Vilakati, B.B. Mamba, Synthesis characterization, and visible light degradation of rhodamine-B dye by carbon-covered alumina supported Pd-TiO_2/polysulfone membranes, Sep. Sci. Technol., 49(14) (2014) 2124–2134.
[9] K.S. Sri, A.K. Nair, P.E. Jagadeesh Babu, Synthesis and characterization of silver decorated polysulfone/cellulose acetate hybrid ultrafiltration membranes using functionalized TiO_2 nanoparticles , Desal. Water Treat., 76 (2017) 112–120.
[10] N.A.A. Hamid, A.F. Ismail, T. Matsuura, A.W. Zularisam, W.J. Lau, E. Yuliwati, M.S. Abdullah, Morphological and separation performance study of polysulfone/titanium dioxide (PSF/TiO_2) ultrafiltration membranes for humic acid removal, Desalination, 273 (2011) 85–92.
[11] R. Kumar, A.M. Isloor, A.F. Ismail, S.A. Rashid, A. Al Ahmed, Permeation, anti fouling and desalination performance of TiO_2

nanotube incorporated PSf/CS blend membranes, Desalination, 316 (2013) 76–84.
[12] A.K. Nair, P.M. Shalin, P.E. Jagadeesh Babu, Performance enhancement of polysulfone ultrafiltration membrane using TiO_2 nanofibers, Desal. Water Treat., 57 (2016) 10506–10514.
[13] S.D. Neelapala, A.K. Nair, P.E. JagadeeshBabu, Synthesis and characterisation of TiO_2 nanofibre/cellulose acetate nanocomposite ultrafiltration membrane, J. Exp. Nano sci., 12 (2017) 152–165.
[14] V. Vatanpour, S.S. Madaeni, A.R. Khataee, E. Salehi, S. Zinadini, H.A. Monfared, TiO_2 embedded mixed matrix PES nanocomposite membranes: Influence of different sizes and types of nanoparticles on anti fouling and performance, Desalination, 292 (2012) 19–29.
[15] A.K. Nair, P.E. JagadeeshBabu, TiO_2 nanosheet-graphene oxide based photocatalytic hierarchical membrane for water purification, Surface coatings Technology., 320 (2017) 259–262.
[16] X.H. Yang, Z. Li, G. Liu, J. Xing, C. Sun, H.G. Yang, C. Li, Ultra-thin anatase TiO_2 nanosheets dominated with {001} facets : thickness-controlled synthesis, growth mechanism and water-splitting properties, Cryst. Eng. Comm., 13 (2011) 1378–1383.
[17] R. Kumar, A.M. Isloor, A.F. Ismail, T. Matsuura, Performance improvement of polysulfone ultrafiltration membrane using N-succinyl chitosan as additive, Desalination, 318 (2013) 1–8.
[18] K. Chen, Z. Jiang, J. Qin, Y. Jiang, R. Li, H. Tang, X. Yang, Synthesis and improved photocatalytic activity of ultra thin TiO_2 nanosheets with nearly 100% exposed (001) facets, Ceram. Int., 40 (2014) 16817–16823.
[19] A.K. Nair, B.V. Kumar, P.E. Jagadeeshbabu, Photocatalytic degradation of Congo red dye using silver doped TiO_2 Nanosheets, in: I. Regupathi, K.V. Shetty, T. Murugesan (eds.), Recent Advances Chemical Engineering, 2016, pp. 211–217.
[20] A.K. Nair, A.M. Isloor, R. Kumar, A.F. Ismail, Anti fouling and performance enhancement of polysulfone ultrafiltration membranes using $CaCO_3$ nanoparticles , Desalination, 322 (2013) 69–75.
[21] S. Zhao, Z. Wang, X. Wei, B. Zhao, J. Wang, Performance improvement of polysulfone ultrafiltration membrane using PANiEB as both pore forming agent and hydrophilic modifier, J. Membr. Sci., 385–386 (2011) 251–262.
[22] Y. Masuda, K. Kato, Synthesis and phase transformation of TiO_2 nano-crystals in aqueous solutions, J. Ceram. Society Japan, 117 (2009) 373–376.
[23] Y. Yang, H. Zhang, P. Wang, Q. Zheng, J. Li, The influence of nano-sized TiO_2 fillers on the morphologies and properties of PSF UF membrane, J. Membr. Sci., 288 (2007) 231–238.
[24] B.M. Ganesh, A.M. Isloor, M. Padaki, Preparation and characterization of polysulfone and modified poly isobutylene-alt-maleic anhydride blend NF membrane, Desalination, 287 (2012) 103–108.
[25] V. Vatanpour, S. Siavash, R. Moradian, S. Zinadini, B. Astinchap, Novel antibifouling nanofiltration polyether sulfone membrane fabricated from embedding TiO_2 coated multi walled carbon nanotubes, Sep. Purif. Technol., 90 (2012) 69–82.
[26] A.L. Ahmad, A.A. Abdulkarim, B.S. Ooi, S. Ismail, Recent development in additives modifications of polyether sulfone membrane for flux enhancement, Chem. Eng. J., 223 (2013) 246–267.
[27] C. Dong, G. He, H. Li, R. Zhao, Y. Han, Y. Deng, Anti fouling enhancement of poly (vinylidene fluoride) microfiltration membrane by adding $Mg(OH)_2$ nanoparticles , J. Membr. Sci., 387–388 (2012) 40–47.
[28] Y. Yang, P. Wang, Q. Zheng, Preparation and properties of polysulfone/TiO_2 composite ultrafiltration membranes, J. Polym. Sci. Part B Polym. Phys., 44 (2006) 879–887.
[29] G. Arthanareeswaran, P. Thanikaivelan, Fabrication of cellulose acetate–zirconia hybrid membranes for ultrafiltration applications: Performance, structure and fouling analysis, Sep. Purif. Technol., 74 (2010) 230–235.
[30] I. Nurul, H. Mohd, A. Wahab, Adsorptive fouling of organic solutes simulating sweet water solutions on ultrafiltration membranes, Chem. Eng. J., 264 (2015) 470–478.
[31] E. Kordouli, K. Bourikas, A. Lycourghiotis, C. Kordulis, The mechanism of azo-dyes adsorption on the titanium dioxide surface and their photocatalytic degradation over samples with various anatase/rutile ratios, Catal. Today. 252 (2015) 128–135.